Self-Indication Resonance Neutron Experiments with Silver (2−200 ev)*

JAMES E. DRAPER†
Brookhaven National Laboratory, Upton, New York, and Yale University, New Haven, Connecticut
(Received June 5, 1958; revised manuscript received January 19, 1959)

A method is given for the area analysis of resonance neutron self-indication experiments including consideration of the effects of energy resolution, wing area, energy dependence of neutron flux, v^{-1} term in the capture cross section, potential scattering, detailed treatment of Doppler broadening, and scattering events preceding capture in the detector sample. The essential result of this measurement alone is nearly the peak total cross section of the Doppler broadened resonance (*viz.*, $\sigma_{t0}\Psi_0/\Psi_0^{\frac{1}{2}}$) which with approximate knowledge of Γ gives σ_{tc}. Experimental results are given for eleven resonances below 200 ev in silver, and they are compared with results obtained by other methods.

THE majority of experiments to measure the Breit-Wigner parameters of neutron resonances have employed neutron detectors whose sensitivity was essentially constant over a resonance. At low-neutron energies where the experimental resolution is good enough to measure the detailed shape, the peak cross section σ_{t0} and the width Γ can be obtained. At higher energies only the area above a transmission dip can usually be obtained which involves both the height and width of the resonance. However, σ_{t0} and Γ can often be separated through the dependence of the area on sample thickness. For self-indication experiments the detector has a resonance response, and it can be shown that in the limit of thin samples the area analysis of such an experiment[1] gives just the peak cross section of the Doppler broadened resonance.

Since effectively thin samples are difficult to employ experimentally the above idealized analysis must be extended to include thicker samples. Anticipating the result shown in Fig. 3, it will be seen that the measurement still gives essentially the peak cross section of the Doppler broadened resonance, but with thicker samples a weak dependence on the width Γ of the resonance is also introduced. The first experiment of this type on the 5.2-ev resonance in silver using time-of-flight techniques has been reported[2] together with the method of analysis. A subsequent analysis[3] considers also the situation where the detector sample and absorber sample are not the same thickness and concludes that the case of equal thicknesses is a reasonable choice. Recently results have been reported from the high-resolution Nevis spectrometer[4] empolying resonance detection for the location of resonances and the use of self-indication methods. In reference 4 the Nevis resonance parameters are tabulated for silver above 100 ev and tantalum above 60 ev, but the methods of analysis of self-indication experiments are not described. Since a full description of the area analysis of self-indication experiments, including corrections, has not been published, this will be considered before describing the present experiments and results.

BASIC FORMULATION

In the first experimental configuration, a foil of the material of interest is placed at the detector position, no foil is in the absorber position, and the (n,γ) processes in the detector foil are recorded by gamma-ray detectors near the foil as represented in the upper curve of Fig. 1. In the second figuration, the counting rate *vs* delay time is repeated with the addition of a foil of the same composition and thickness placed about midway between the neutron source and the detector foil. The result is the lower curve of Fig. 1. The analysis of the data will first be outlined in terms of a simplified form of the Breit-Wigner single-level expression modified by Doppler broadening of the resonance. Then there are incorporated the corrections for the more detailed form of the resonance shape and neutron flux, for neutron energy resolution, and for multiple neutron events in the detector foil. The most important effect which is not considered is the inadequacy of the single-level resonance expression.

The Breit-Wigner capture cross section in the vicinity of the resonance energy can be written as

$$\sigma_{c0}(1+x^2)^{-1}(1+\gamma x)^{-\frac{1}{2}}, \tag{1a}$$

and the scattering cross section as

$$\sigma_{s0}(1+x^2)^{-1}[1+2\Gamma Rx/\Gamma_n\lambda\!\!\!^{-}_0]+\sigma_p, \tag{1b}$$

where

$$\sigma_{c0}=\sigma_{t0}\Gamma_\gamma/\Gamma,\quad \sigma_{s0}=\sigma_{t0}\Gamma_n/\Gamma,\quad \sigma_{t0}=g4\pi\lambda\!\!\!^{-}_0{}^2\Gamma_n/\Gamma,$$
$$x=(2/\Gamma)(E-E_0),\quad \gamma=\Gamma/2E_0,\quad \sigma_p=4\pi R^2,$$

and

$$2g=1\pm(2I+1)^{-1}.$$

E is the neutron energy, $2\pi\lambda\!\!\!^{-}_0$ is the wavelength of a neutron of the resonance energy, E_0, R is the radius of the nucleus and Γ_n, Γ_γ, and Γ are the neutron, radiation, and total widths of the level at resonance.

* Work performed under contract with the U. S. Atomic Energy Commission.
† Present address: Yale University, New Haven, Connecticut.
[1] H. A. Bethe, Revs. Modern Phys. **9**, 141 (1937).
[2] J. E. Draper and C. P. Baker, Phys. Rev. **95**, 644(A) (1954).
[3] E. Melkonian, *Proceedings of the International Conference on the Peaceful Uses of Atomic Energy, Geneva, 1955* (United Nations, New York, 1956), Vol. 4, p. 347.
[4] J. Rainwater, *Handbuch der Physik* (Springer-Verlag, Berlin, 1957), Vol. 40, p. 373.

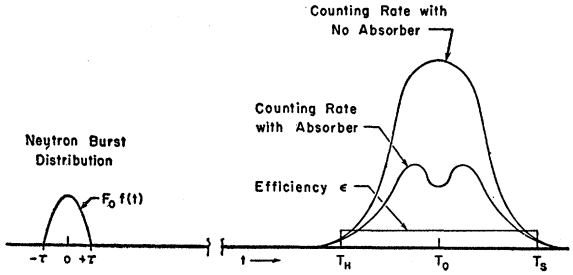

FIG. 1. Schematic representation of the self-indication experiment. The function $f(t)$ represents the shape of the neutron burst of duration 2τ and is used to evaluate the effect of energy resolution. The curves on the right represent the response of the resonance detector with, and without, a resonance absorber of the same thickness placed midway along the beam. The detector efficiency ϵ is assumed constant between the two cutoffs T_H and T_S. The horizontal distance relates the time elapsed after the center of the neutron burst.

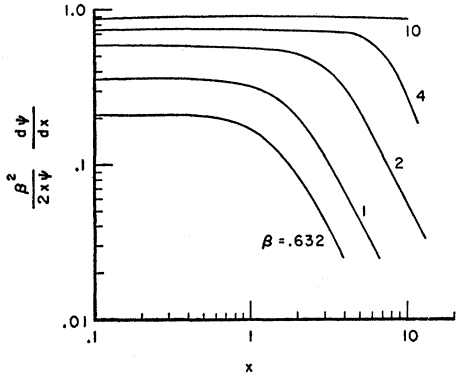

FIG. 2. The Doppler correction factor $(\beta^2/2x\Psi)(d\Psi/dx)$ in Eqs. (3) which modifies the interference term in the scattering cross section and modifies the (velocity)$^{-1}$ term in the capture cross section.

When the cross sections in expressions (1) are approximated by setting $\gamma=0$ and $R=0$ the Doppler function $\Psi(\beta,x)$ is obtained which is

$$\Psi(\beta,x)=\frac{1}{\beta\pi^{\frac{1}{2}}}\int_{-\infty}^{\infty}dy\frac{1}{1+y^2}\exp[-(x-y)^2/\beta^2], \quad (2)$$

where

$$\beta=(2/\Gamma)(4E_0kT/M)^{\frac{1}{2}}, \quad (2a)$$

M is the ratio of the mass of the target nucleus to the mass of the neutron, k is Boltzmann's constant and T is the temperature prescribed by Lamb[5] for a Debye solid. The function $\Psi(\beta,x)$ has been evaluated[6] and tabulated.[7,8] The notation Ψ_0 will represent $\Psi(\beta,0)$.

When the complete expressions (1a) and (1b) are used in place of $(1+y^2)^{-1}$ in Eq. (2) the more exact Doppler broadened cross sections can be shown to be

$$\sigma_s=\sigma_{s0}\Psi\{1+[2\Gamma Rx/\Gamma_n\lambda_0]\times[1+(\beta^2/2x\Psi)(d\Psi/dx)]\}, \quad (3a)$$

and for $\gamma x\ll 1$

$$\sigma_c=\sigma_{c0}\Psi(1+\gamma x)^{-\frac{1}{2}}[1-(\gamma x/2)(1+\gamma x)^{-1}\times(\beta^2/2x\Psi)(d\Psi/dx)+\cdots]. \quad (3b)$$

The Doppler broadened total cross section is

$$\sigma_t+\sigma_p=\sigma_c+\sigma_s+\sigma_p. \quad (3c)$$

The quantity $(\beta^2/2x\Psi)(d\Psi/dx)$ was calculated from reference 8 and is plotted in Fig. 2.

Define A and B as

$$A=(\Gamma/2)\int_{-\infty}^{\infty}dx(1-e^{-N\sigma_{t0}\Psi})(\sigma_{c0}\Psi/\sigma_{t0}\Psi), \quad (4a)$$

and

$$B=(\Gamma/2)\int_{-\infty}^{\infty}dx\,e^{-N\sigma_{t0}\Psi}(1-e^{-N\sigma_{t0}\Psi})(\sigma_{c0}\Psi/\sigma_{t0}\Psi), \quad (4b)$$

where N is the number of nuclei cm^{-2} in the detector foil and the absorber foil is of the same thickness. These integrands are closely related to the curves of Fig. 1, and they represent the rate of capture of neutrons in the foils in the energy interval $(\Gamma/2)dx$ under the following hypothetical conditions: only single interactions of neutrons occur in the detector foil; $R=0$ in Eq. (3a); $\gamma x\ll 1$ in Eq. (3b) (i.e., $|E-E_0|/E_0\ll 1$); unit incident neutron flux for all energies in the vicinity of the resonance. These restrictions will later be removed.

Consider now the ratio B/A. Rearrangement of (4b) and combination with (4a) will show that

$$B(N)=A(2N)-A(N). \quad (5)$$

Equation (5) is also given in references (2) and (3). $A(N)$ is related by the factor Γ_γ/Γ to the area above a transmission dip in the more familiar transmission experiments with a nonresonant detector (e.g., BF_3 counters). This area, including the effect of Doppler broadening, has been calculated, (recently summarized in reference 4) and the results have been combined with Eq. (5) to obtain B/A as presented[9] in Fig. 3. The graph of Fig. 3 will furnish the link between the data obtained from self-indication experiments and the peak total cross section.

CORRECTIONS

A. Experimental Resolution

The duration of the neutron burst is not always negligible compared with $|T_S-T_H|$ of Fig. 1. This will affect the area by modifying the effective cutoff T_S and T_H. In Fig. 1 $F_0f(t)$ is the emission rate of neutrons

[5] W. E. Lamb, Jr., Phys. Rev. **55**, 190 (1939).
[6] M. Born, *Optik* (Verlag Julius Springer, Berlin, 1933), p. 482.
[7] Rose, Miranker, Leak, and Rabinowitz, Brookhaven National Laboratory Report BNL-257, 1953 (unpublished).
[8] Rose, Miranker, Leak, Rosenthal, and Hendrickson, Westinghouse Electric Comporation Atomic Powers Division Report, WAPD-SR-506, 1955 (unpublished).
[9] Part of the curves for $\beta=0$ and $\beta=10$ are shown in reference 3, and some of the curves were presented in reference 2.

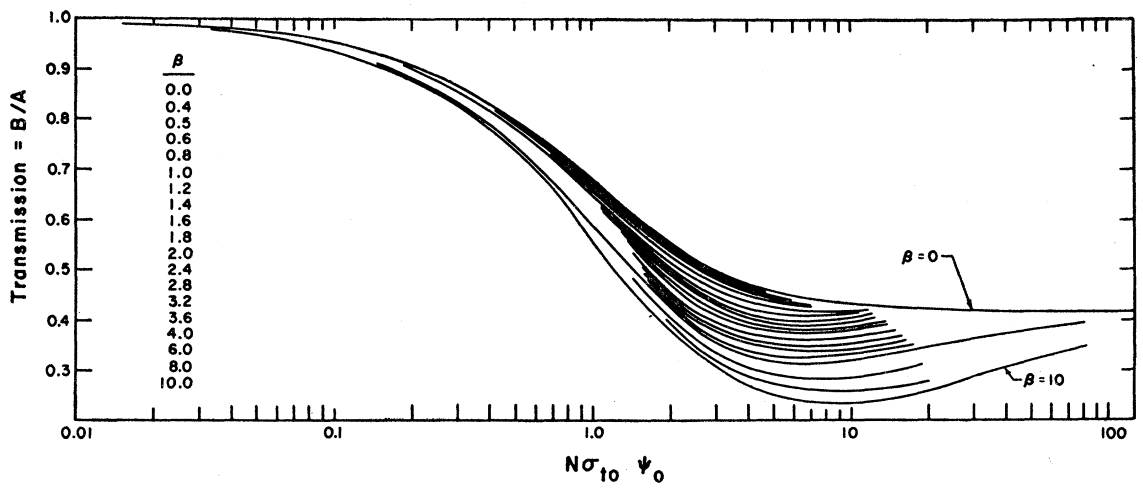

FIG. 3. The self-indication transmission discussed after Eq. (5) in terms of the peak Doppler broadened cross section. The areas B and A are closely related to those of Fig. 1 but involve the idealized cross sections of Eq. (4).

during the burst. It is assumed that $f(t)$ is adequately represented by the sum of a symmetric function $f_+(t)$ and an antisymmetric function $f_-(t)$. The time integral of $f(t)$ is unity. The detector gates are considered rectangular and for area analysis the counts arising between T_H and T_S are summed. The quantity ϵ is the detector efficiency. T_H and T_S are selected such that the height of the top curve in Fig. 1 at T_H or T_S is less than $\frac{1}{10}$ of the central height, while keeping $|E-E_0|<E_0/2$ within the interval T_H to T_S.

Define A_{x0} as the total number of captured neutrons in the time interval between T_H and T_S (no absorber present) for unit neutron flux at time T_0. The value of A_{x0} will depend on the width of the neutron burst. For an infinitesimal burst width the value of A_{x0} is defined as A_D so that

$$A_D=(\Gamma/2)\int_{-S}^{H}dx[1-e^{-N\sigma_t-N\sigma_p}]\times[\sigma_c/(\sigma_t+\sigma_p)](E_0/E), \quad (6)$$

where H is the magnitude of x at T_H, and S is the magnitude of x at T_S. The factor E_0/E represents the energy dpendence of the neutron flux from the moderator. The cross sections are those of Eq. (3).

The effects of the nonzero neutron source burst width are contained in a_r defined by $A_{x0}=A_D-a_r(N\sigma_{t0}\Gamma_\gamma)$. The analysis of a_r will not be given but the result is

$$a_r=(\kappa\mu/W)\left[\frac{4}{3}\nu\rho_+\frac{\tau^2}{(T_S-T_H)^2}+\frac{2}{3}\kappa\frac{H-S}{W}\rho_-\frac{\tau}{|T_S-T_H|}\right], \quad (7)$$

where $2W\equiv H+S$,

$$\rho_+=6\int^{\tau}dt(t/\tau)^2f_+(t),\qquad \rho_-=6\int_0^{\tau}dt(t/\tau)f_-(t), \quad (7a)$$

and τ is shown in Fig. 1. A representative burst shape $f(t)$ gives $\rho_+=1$ and $\rho_-=0.1$. The constants κ, μ, and ν are each ~1 and are defined as

$$\kappa=\left|\frac{E_H-E_S}{T_S-T_H}\left(\frac{dt}{dE}\right)_{E_0}\right|,\qquad \mu=\left|\frac{d\Psi}{dx}\right|_{x=W}\frac{W^3}{2}\left[1+\frac{9}{4}\frac{|T_S-T_H|}{T_0}\right]^{-1}, \quad (7b)$$

and

$$\nu=\left[\left|\frac{d\Psi}{dx}(1+\gamma x)^{\frac{3}{2}}\right|_{x=H}+\left|\frac{d\Psi}{dx}(1+\gamma x)^{\frac{3}{2}}\right|_{x=S}\right]\left[2\left|\frac{d\Psi}{dx}\right|_{x=W}\right]^{-1}.$$

The correction term a_r is generally small because $\tau\ll|T_H-T_S|$ at low energy where a resonance covers many channels, and at high energies W becomes large (i.e., the poorer resolution forces the cutoff farther into the wings). If the cutoff is symmetrical in energy then the second term of a_r vanishes.

For the case with the absorber present, B_{x0} is the analog of A_{x0} for the lower curve of Fig. 1 and B_D is defined as

$$B_D=(\Gamma/2)\int_{-S}^{H}dx\,e^{-N\sigma_t-N\sigma_p}[1-e^{-N\sigma_t-N\sigma_p}]\times[\sigma_c/(\sigma_t+\sigma_p)](E_0/E). \quad (8)$$

A similar analysis shows $B_{x0}=B_D-a_rN\sigma_{t0}\Gamma_\gamma$ where a_r is the same for A_{x0} and B_{x0} because $N(\sigma_t+\sigma_p)\ll 1$ near cutoff. This completes the relation between the experimental areas A_{x0} and B_{x0} and the areas A_D and B_D which would be obtained with a neutron burst of zero width.

B. Contribution of Wings, of Departure from Idealized Cross Section and of Energy Dependence of Flux

The quantities A and B of Eq. (4) contain the essential features of the cross sections which are pertinent to area analysis with the resonant capture detector. However, the idealized cross sections in A and B differ from the actual cross sections in Eq. (3). In addition, the contributions of the wings of the resonance must be considered in relating the quantities A_D and B_D to A and B.

In order to compare the two integrands define

$$I=[1-e^{-N\sigma_t-N\sigma_p}][\sigma_c/(\sigma_t+\sigma_p)](E_0/E), \quad (9a)$$

and

$$I_0=[1-e^{-N\sigma_{t0}\Psi}](\sigma_{c0}/\sigma_{t0}). \quad (9b)$$

Then A and B of Eq. (4) contain I_0 while A_D and B_D of Eqs. (6) and (8) contain I.

By separating these integrals into various parts the identity

$$A=A_D+(a_w+a_v)N\sigma_{t0}\Gamma_\gamma, \quad (10)$$

results, where a_w is defined by

$$a_w=(N\sigma_{t0}\Gamma_\gamma)^{-1}\left\{(\Gamma/2)\int_{-\infty}^{-S}dxI_0+(\Gamma/2)\int_H^\infty dxI_0\right\}, \quad (10a)$$

and a_v is defined by

$$a_v=(N\sigma_{t0}\Gamma_\gamma)^{-1}(\Gamma/2)\int_{-S}^{H}dx(I_0-I). \quad (10b)$$

Consider first the wing correction a_w under the assumption that $N(\sigma_t+\sigma_p)\ll 1$ for $E<E_S$ and for $E>E_H$. In order to simplify the expression for a_w, define $\omega(H)$ by

$$\int_H^\infty dx\Psi(\beta,x)=[1+\omega(H)]/H. \quad (11)$$

Values of $\omega(H)$ are plotted against H/β in Fig. 4 and were obtained by numerical integration. Then

$$a_w=\frac{1+\omega(H)}{2H}+\frac{1+\omega(S)}{2S}. \quad (12)$$

The evaluation of a_v is more complicated. It contains the effects of the (velocity)$^{-1}$ factor in the capture cross section, the E_0/E factor in the neutron flux, the effect of potential scattering and the extra terms in σ_s and σ_c in Eq. (3). Fortunately, it is often an unimportant correction. The quantity a_v is estimated as

$$a_v=\frac{\sigma_p}{\sigma_{t0}}\left[\frac{U}{3}+\frac{\gamma H-\gamma S}{2}\left(1-\frac{\Gamma_n}{\Gamma}-2j\right)\right]-\frac{\gamma}{\Psi_0}\left[\frac{11}{16}(\gamma H+\gamma S)\left(1+\frac{2}{11}\frac{\Gamma_n}{\Gamma}+\frac{4j}{11}+\frac{6d_0}{11}\right)-\tfrac{3}{8}\ln\left(\frac{\Psi(\beta,S)}{\Psi(\beta,H)}\right)\right], \quad (13)$$

where U is the value of $|x|$ for which $N\sigma_t=1$ and is defined as $U=0$ if $N\sigma_{t0}\Psi_0\leqslant 1$. The quantity d_0 is the limiting value of $(\beta^2/2x\Psi)(d\Psi/dx)$ in Fig. 2 as $x\to 0$ and the quantity $j=2R/\gamma\lambda_0$. If a more accurate value of a_v is required it must be obtained by numerical integration of the functions I and I_0 with the actual parameters of interest. However Eq. (13) will usually serve to show that a_v is negligible.

By reference to Eqs. (5) and (10) it can be shown that the equation analogous to Eq. (10) is

$$B=B_D+[a_w+a_v(2N)-a_v(N)]N\sigma_{t0}\Gamma_\gamma \quad (14)$$

for the case with the absorber present.

In order to clarify the final results some notational changes follow. Denote A_0 as the value of A in Eq. (4a)

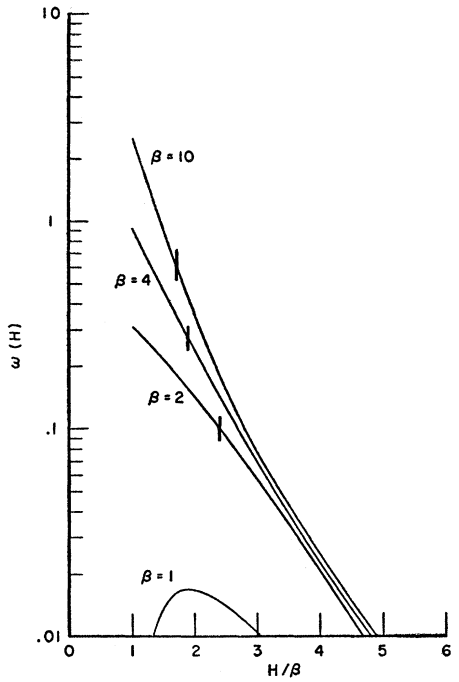

FIG. 4. The quantity $\omega(H)$ which must be incorporated in the wing correction a_w of Eqs. (10) and (11), plotted in terms of the value H of $x=(E-E_0)2/\Gamma$ at the cutoff. The vertical dashes, for reference, denote the value of H where $\Psi(\beta,H)=0.1\Psi(\beta,0)$.

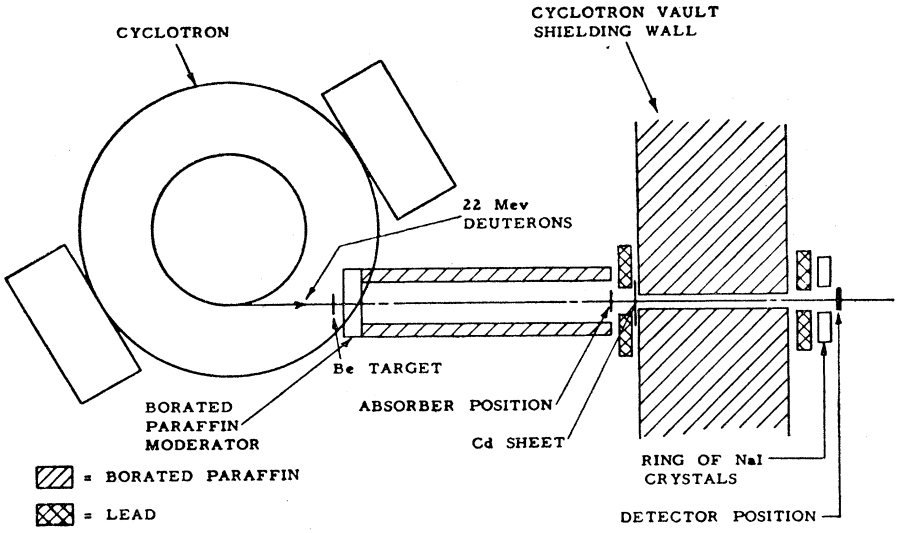

FIG. 5. Schematic geometry. The detector was a foil of silver viewed by six NaI(Tl) scintillators in multiple twofold coincidence. The flight path was 4.3 m.

for $\beta=0$—i.e.,

$$A_0=(\Gamma_\gamma/2)\int_{-\infty}^{\infty}dx\{1-\exp[-N\sigma_{t0}/(1+x^2)]\}. \quad (15a)$$

This function has been evaluated.[10,11] Define $D(N\sigma_{t0},\beta)$ by

$$A=A_0(1+D), \quad (15b)$$

so that D contains the influence of Doppler broadening as evaluated by Melkonian.[12] Further define δ_A and δ_B by

$$\delta_A=(a_r+a_w+a_v)N\sigma_{t0}\Gamma_\gamma/A_0(1+D), \quad (16a)$$

and

$$\delta_B=(A/B)\{\delta_A+[a_v(2N)-2a_v(N)]\times N\sigma_{t0}\Gamma_\gamma/A_0(1+D)\}. \quad (16b)$$

Then combining the previous results

$$A=A_{x0}/(1-\delta_A), \quad (17a)$$

and

$$B=B_{x0}/(1-\delta_B), \quad (17b)$$

where $F_0\epsilon A_{x0}$ and $F_0\epsilon B_{x0}$ were defined earlier as the areas under the curves of Fig. 1 between T_H and T_S.

C. Corrections for Multiple Interactions of Neutrons

To this point it has been approximated that a neutron interacts no more than once in the detector foil. However, when the foils are not very thin there can be an appreciable contribution to the neutron capture rate from neutrons which scatter before being captured.

If there were no multiple interactions the equations

$$A=A_{x0}+[a_r+a_w+a_v]N\sigma_{t0}\Gamma_\gamma, \quad (18a)$$

and

$$B=B_{x0}+[a_r+a_w+a_v(2N)-a_v(N)]N\sigma_{t0}\Gamma_\gamma \quad (18b)$$

would apply. When multiple interactions are "turned on," these become

$$A(1+m_A)=A_x+(1+m_A)[a_r+a_w+a_v]N\sigma_{t0}\Gamma_\gamma, \quad (18c)$$

and

$$B(1+m_B)=B_x+(1+m_B)[a_r+a_w+a_v(2N)-a_v(N)]N\sigma_{t0}\Gamma_\gamma. \quad (18d)$$

Here A_x is defined as the value that A_{x0} assumes in the presence of multiple interactions and m_A is defined by Eq. (18c). Similarly B_x is defined as the value that B_{x0} assumes in the presence of multiple interactions and m_B is defined by Eq. (18d).

The values of m_A and m_B have been evaluated[13] as

$$1+m_A=1+\frac{\gamma_n q}{1-\gamma_n q}+\frac{Q_{2p}/Q_1}{1-Q_{2p}/Q_1}, \quad (19a)$$

and

$$\frac{1+m_B}{1+m_A}=1-\frac{\gamma_n qr}{1-\gamma_n q(1-r)}-\left[\frac{Q_{2p}}{Q_1}-\frac{Q_{2pA}}{Q_{1A}}\right], \quad (19b)$$

where $\gamma_n=\Gamma_n/\Gamma$ and the quantities q, r, Q_{2p}, Q_1, Q_{2pA}, and Q_{1A} are calculated and presented in graphical form in reference 13.

ANALYSIS

With the incorporation of multiple interactions the final results are

$$A=A_x(1-\delta_A)^{-1}(1+m_A)^{-1}, \quad (20a)$$

and

$$B=B_x(1-\delta_B)^{-1}(1+m_B)^{-1}. \quad (20b)$$

[10] R. Ladenburg and F. Reiche, Ann. Physik **42**, 181 (1913).
[11] G. von Dardel and R. Persson, Nature **170**, 1117 (1952).
[12] Melkonian, Havens, and Rainwater, Phys. Rev. **92**, 702 (1953).
[13] J. E. Draper, Nuclear Sci. and Eng. **1**, 522 (1956).

Equations (20) now represent the desired final relation between the data, A_x and B_x, and the quantities A and B to be used with Fig. 3 for analysis of the peak cross section. They are employed by iteration in which B_x/A_x is first used (with Γ approximated as Γ_γ) to obtain approximate resonance parameters with which to calculate δ_A, δ_B, m_A, and m_B. The resultant B/A may be used in the next approximation, but this step is usually unnecessary.

Having determined B/A, the choice of the curve from the family in Fig. 3 is dictated by β—i.e., Γ. While the resulting peak Doppler cross section $\sigma_{t0}\Psi_0$ is rather insensitive to the choice of Γ, it can be shown graphically with Fig. 3 that $\sigma_{t0}\Psi_0/\Psi_0^{\frac{1}{3}}$ is even less sensitive, being independent of the choice of Γ (within $\pm 9\%$) for $0 \leqslant \beta \leqslant 5$ and $N\sigma_{t0}\Psi \leqslant 3$. Consequently, $\sigma_{t0}\Psi_0/\Psi_0^{\frac{1}{3}}$ will be quoted as the most direct experimental result of self-indication area analysis alone, and the approximation $\Gamma \approx \Gamma_\gamma$ will usually give sufficient accuracy for this result. This must be combined with another type of measurement such as a thick sample transmission measurement of $\sigma_{t0}\Gamma^2$ to obtain σ_{t0} and Γ separately. It is apparent from Fig. 3 that a sufficiently accurate set of values of B/A including values near the minima would determine β and thus both σ_{t0} and Γ would be determined. However, the required accuracy for B/A would unduly emphasize the corrections for multiple neutron interactions and the corrections for gamma-ray absorption in the detector sample for sample thicknesses of $N\sigma_{t0}\Psi_0 \sim 10$ where those corrections become significant.

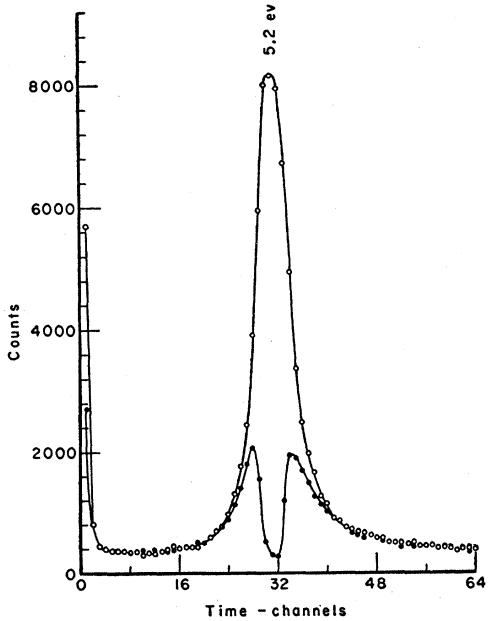

FIG. 6. Self-indication data for the neutron energy range 2.3–16 ev using silver detector and absorber foils each of 0.327 g/cm². The upper curve was obtained without an abosrber foil, and for the lower curve the abosrber foil was interposed. The channel width was 2 μsec. No background has been subtracted.

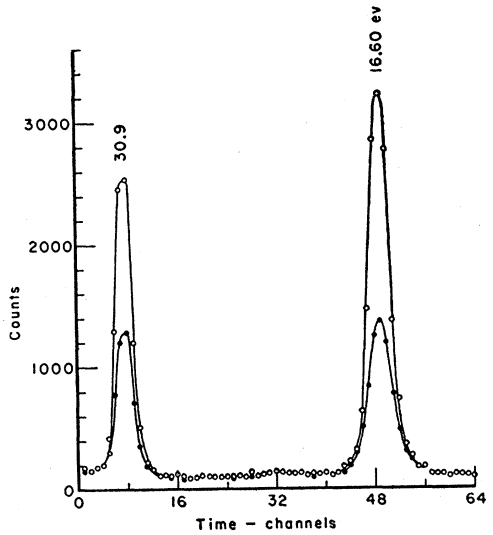

FIG. 7. Similar to Fig. 6 but covering the neutron energy range 14–35 ev. The channel width was 0.5 μsec.

EXPERIMENTAL METHOD AND DATA

Figure 5 shows the experimental geometry. The arc of the cyclotron was pulsed to produce 0.6-μsec bursts of 22-Mev deuterons at intervals of 700 μsec. The instantaneous beam current of 1 milliamp at the external beryllium target (averaged over an rf period) produced a calculated average neutron output[14] of 10^{11} neutrons during each second. The cyclotron pulsing equipment has been described.[15] The neutrons were moderated in a 2-in. slab of paraffin. The moderation time produced a time uncertainty which can be expressed[16] as an uncertainty in flight path of ~ 2 mean-free-paths in paraffin or 1–2 cm.

The detector consisted of a foil of the material of interest viewed by a ring of six NaI(Tl) scintillators, each 4-cm diam. by 3 cm. The diameter of the collimation hole through the shielding wall was 2.5 in. and the front face of each NaI scintillator was located on a circle of 4-in. diameter. The flight path was 4.3 m.

In order to reduce the relative contribution of background, coincidences were required from the scintillators. That is, a neutron capture event was recorded if it produced a two-fold coincidence between any of the 15 possible pairs of the 6 scintillators. Thus if the cascade gamma-ray average multiplicity[17] is ν and the average detector efficiency of one scintillator is $\epsilon \ll 1$, then the ratio of coincidence counting rate with 6 scintillators to the counting rate from one of the scintillators is $15(\nu-1)\epsilon \sim 1$. It will be apparent from Figs. 6–8 that the large ratio of foreground to background counting rate even with thin samples greatly

[14] L. W. Smith and P. G. Kruger, Phys. Rev. **83**, 1137 (1951); Allen, Nechaj, Sun, and Jennings, Phys. Rev. **81**, 536 (1951).
[15] J. E. Draper, Rev. Sci. Instr. **29**, 137 (1958).
[16] H. Groenewald and H. Groendijk, Physica **13**, 141 (1947).
[17] C. O. Muehlhause, Phys. Rev. **79**, 277 (1950).

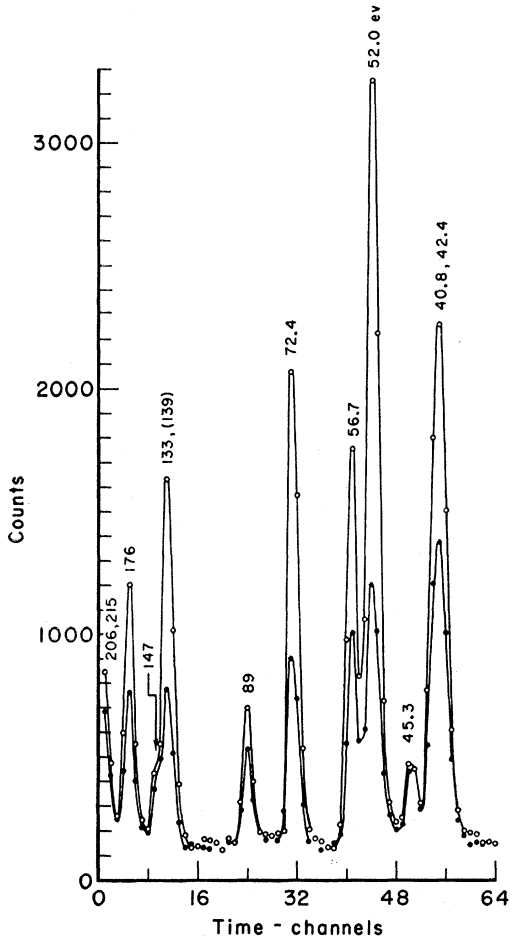

FIG. 8. Similar to Fig. 6 but covering the neutron energy range 34–215 ev. The channel width was 0.5 μsec.

reduces the uncertainty in determining the total number of counts due to a resonance.

The coincidences were provided by delivering the output of the six photomultipliers through six preamplifiers of gain 2.5 to six Hewlett-Packard distributed amplifiers and then to six EFP60 trigger circuits. The negative pulse from each trigger circuit was fed to one of six 6AK5 tubes whose plates were joined and connected through 15 ft of 200-ohm coax cable to the $B+$ supply (with the cable shorted at the $B+$ end). A crystal diode discriminator at the output of the common plates was then set to record any pulse whose height corresponded to the cutting off of more than one of the 6AK5 tubes within a time interval equal to the 0.04-μsec round-trip time of the shorted coax cable in the plate circuit. The bias level for this detection system was set at a gamma-ray energy of 75 kev.

The resulting coincidence pulses were analyzed in a conventional 64-channel time analyzer. The block of 64 channels could be delayed by an interval from 4 to 1024 μsec after the cyclotron pulse. The analyzer channel width of 0.5 μsec was obtained from a gated

TABLE I. Summary of correction terms for the thickest sample—*viz.*, 0.327 g/cm², except 0.0258 g/cm² for the 5.2-ev resonance.

E_0 (ev)	a_r ($\times 10^3$)	a_w ($\times 10^3$)	a_v ($\times 10^3$)	γ_{nq}	BA_x/AB_x
5.20	0.1	111	−11	0.039	1.093
16.6	0.3	67	−0.9	0.013	1.060
30.9	0.6	45	−1.2	0.014	1.051
40.8, 42.4	1.0	48	−0.6	0.010	1.026
52.0	0.6	30	−1.4	0.029	1.033
56.7	1.0	38	−1.2	0.031	1.024
72.4	0.3	16	−1.3	0.031	1.009
89	0.5	16	−0.2	0.008	1.004
133	0.4	15	−1.2	0.058	1.004
176	0.9	17	−1.4	0.053	1.004

2-Mc/sec oscillator which was turned on by the beam pulse at the target of the cyclotron. The analyzer basically consisted of two parallel blocks of 32 channels whose widths were fixed by 32 scaling circuits. Since these were uneven and unstable by ~15% a single 2-Mc/sec scaling circuit was used to fix the 0.5-μsec channel widths and to distribute the incident data pulses alternately between the two blocks of 32 1-μsec channels. The resulting 64 0.5-μsec channel widths were equal and stable to within ±1%.

Examples of the data for neutron energies up to 215 ev are shown in Figs. 6–8. The quantity of interest for each resonance is the ratio B_x/A_x of the areas under the two curves between the cutoff channels. The data of Fig. 6 consist of a total of eight runs—four with the absorber and four without the absorber. The absorber runs and open runs were always alternated in order that any slow drifts of the detection bias and efficiency should have minimal effect. The thicknesses of the detector samples and of the absorber samples were nominally 1, 2, 4, 6, and 12 mils. The silver samples were of 99.9% purity. As shown above the value of $\sigma_{t0}\Psi_0/\Psi_0^{\frac{1}{3}}$ can be obtained with only one pair of measurements using a sample thickness such that B_x/A_x is about 0.6. However, the variety of sample thicknesses required to approximate these conditions for many resonances makes it possible to compare the experimental shape of the plot of B/A *vs* thickness with Fig. 3.

The resonances at 5.2, 16.6, 30.9, 45.3, 52.0, 56.7, 72.4, 89, and 176 ev are sufficiently well resolved for analysis. The peak in the region of 140 ev contains a strong resonance at 133 ev, a weaker resonance at 147 ev, and a very weak resonance[18] at 139 ev. Since the resonances at 40.8 and 42.4 ev are not separated, the average cross section for these two resonances will be obtained. Their resonance energies[18] are separated by more than ten units of Γ, and under the assumption that their peak cross sections and widths are roughly

[18] *Neutron Cross Sections*, compiled by D. J. Hughes and J. A. Harvey, Brookhaven National Laboratory Report BNL-325 (Superintendent of Documents, U. S. Government Printing Office, Washington, D. C., 1955), and D. J. Hughes and R. B. Schwartz, Suppl. No. 1 to BNL-325, 1957.

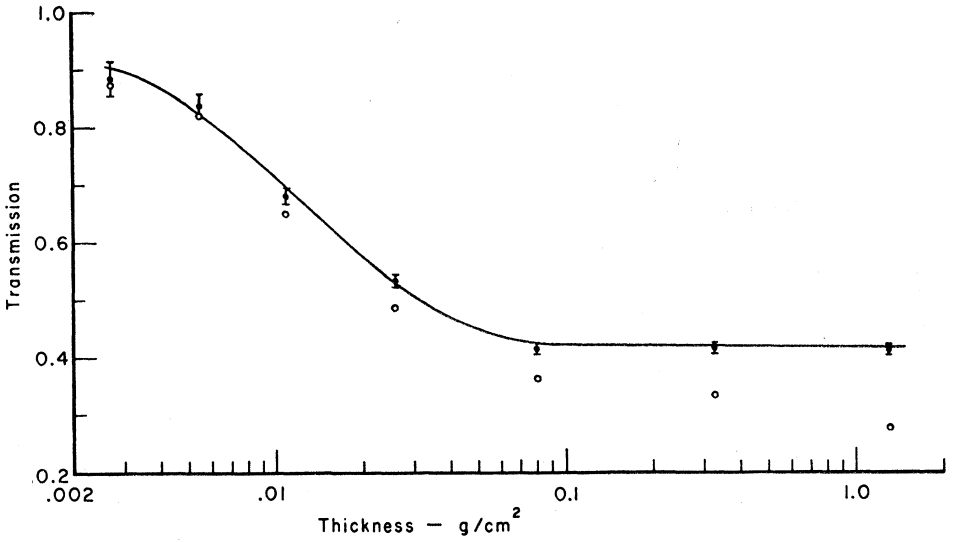

FIG. 9. Comparison of data and theory for the 5.20-ev resonance. The open circles are the uncorrected ratios B_x/A_x. The closed circles are the corrected ratios B/A. The solid curve came from Fig. 3 with $\beta=0.9$. The statistical uncertainty is just the standard deviation deduced from the total number of counts. The samples of thickness greater than 0.03 g/cm² are included to test the validity of the analysis.

the same, the result is the average cross section. The resonance at 147 ev is sufficiently separated to show that it is much weaker than the 133-ev resonance and to subtract its contribution to the 133-ev peak, but it is not sufficiently separated to obtain a good measure of its cross section.

The results of the analysis of the corrections according to the methods above are summarized for a few cases in Table I. The examples cited are for the thickest samples which contribute significantly to the determination of the cross section. In all cases the resulting plots of B/A *vs* sample thickness matched the curve of Fig. 3 within the limitations of the counting statistics. In Fig. 9 is shown a comparison of data with the curve from Fig. 3.

Consider now the possiblility of resonance capture by the iodine in NaI of some of the neutrons scattered from the sample. The effect is negligibly small except when the peak of an iodine resonance is within about 0.2 ev of $E_0[1-\Delta(\theta)]$ which represents the energy of a neutron after scattering from silver through the angle θ, ($\theta\sim120°$), having had the energy E_0 of a resonance peak in silver before scattering. The exact analysis of this problem would be complex, but it is similar to the problem[13] of a neutron being captured in the sample foil after first being scattered there. An analytic estimate of this has been made, the details of which will not be presented here. A comparison of the resonance energies[18] of iodine and of silver indicates that the only significant contribution might be in the 30.9-ev resonance. However, the analytic estimate for the thickest sample indicates that of all counts in the 30.9-ev resonance (upper curve of Fig. 7) the fraction due to this iodine-capture effect is 0.005. A similar fraction contributes to the lower curve. The resulting influence on B_x/A_x has been disregarded.

The correction for absorption of gamma rays by the sample was negligible since the thickest sample was less than 0.1 of a gamma-ray mean free path above 200 kev. In addition, the gamma rays leave the same face of the sample through which the neutrons enter, thus reducing absorption. The infiuence of the 16.6-ev resonance on the 5.2-ev resonance analysis was calculated according to the single-level Breit-Wigner formula. This calculation showed that even for the thickest sample in Fig. 9, the influence of the 16.6-ev resonance was negligible. For that case it changes B/A by 0.005.

EXPERIMENTAL RESULTS

The cross sections are listed in Table II. As described above, the experimental result of the present measurements which is least dependent on the assumed value of Γ is $\sigma_{t0}\Psi_0/\Psi_0^{\frac{1}{2}}$ which is listed in column 2. To determine the quantity $\sigma_{t0}\Psi_0/\Psi_0^{\frac{1}{2}}$ the experimental values of B/A plotted on semilog paper against sample thickness were superposed over Fig. 3 and translated horizontally for best fit. The quoted experimental uncertainty for $\sigma_{t0}\Psi_0/\Psi_0^{\frac{1}{2}}$ was obtained by further horizontal translation until an average (averaged for 5 samples) value of 3.0 was obtained for the square of the following ratio: (difference between the experimental value of B/A and that of Fig. 3)÷(standard deviation obtained from the counting statistics).

In order to compare with experimental results of other measurements the values of σ_{t0} were calculated using the most recently reported values of Γ published[19] by Harwell except that reference 18 was used for the 176-ev resonance. However, it is evident that the magnitude of $\Psi_0^{\frac{1}{2}}$ is not very sensitive to Γ. Since the quoted[19] uncertainties in Γ were less than $\pm15\%$ they had little effect on the uncertainties in σ_{t0}.

The σ_{t0} entered in Table II for the BNL chopper was

[19] Rae, Collins, Kinsey, Lynn, and Wiblin, Nuclear Phys. 5, 89 (1958).

TABLE II. Isotopic cross sections.

E_0 (ev)[a]	This work $\sigma_{t0}\Psi_0/\Psi_0^{\frac{1}{2}}$ (kb)	σ_{t0} in kilobarns[f] BNL chopper[c]	MTR chopper[d]	Nevis[e]	Harwell[g]	This work[h]
5.2[b]	28.6±2	27.3±1	···	···	31.9	34.1±2
16.6	2.4±0.3	2.9	2.7±0.7	···	3.2	3.5±0.4
30.9	2.2±0.3	2.3	3.5±0.6	3.9	2.8	3.4±0.4
40.8	1.3±0.2	1.7	1.6	2.2	1.7	2.2±0.3
42.4		2.2	1.8	2.3		
52.0	3.2±0.4	6.1	6.4±1.4	6.9	5.0	5.5±0.7
56.7	1.8±0.3	2.9	1.3±0.5	2.8	2.3	3.0±0.4
72.4	3.5±0.6	4.2	8.5±1.9	4.3	3.9	6.1±1
89	$0.8^{+0.7}_{-0.4}$	0.8	0.56	···	0.85	$1.6^{+1.4}_{-0.8}$
133	3.0±0.4	···	5.6	4.8	6.8	5.7±0.6
176	1.8±0.5	···	2.8	3.1	···	2.9±0.8

[a] See reference 18 for resonance energies and isotopic assignments.
[b] R. E. Wood [Phys. Rev. **104**, 1425 (1956)] quotes $\sigma_{t0}=34\pm1$ kb for the 5.20-ev resonance. See also reference 2.
[c] Composite of BNL values[20] of $\sigma_{t0}\Gamma^2$ and Harwell values[19] of Γ except for the 5.2-ev resonance where σ_{t0} is quoted.
[d] Calculated from published[21] values of E_0, $g\Gamma_n$, and Γ_γ, except that those with experimental uncertainties were quoted as σ_{t0}.
[e] The first six are calculated from reported values[22] of $\sigma_{t0}\Gamma^2$ and the Harwell values[21] of Γ. The last two are taken from that part of Table I, reference 4 which is attributed to Nevis.
[f] Experimental uncertainty of other authors is listed only when σ_{t0} is quoted directly.
[g] Calculated from the reported values [19] of E_0, g, Γ_n, and Γ.
[h] Calculated from $\sigma_{t0}\Psi_0/\Psi_0^{\frac{1}{2}}$ and Harwell values[19] of Γ except the 176-ev resonance.[18]

obtained from the $\sigma_{t0}\Gamma^2$ of Seidl *et al.*[20] and the Γ of reference 19 since only approximate values of Γ can be obtained from reference 20. Since the σ_{t0} derived from $\sigma_{t0}\Gamma^2$ is quite sensitive to Γ, this procedure was avoided wherever possible but was necessary for column 3 and part of column 5 of Table II. For the MTR chopper[21] when σ_{t0} was not quoted it was calculated from their values of E_0, $g\Gamma_n$, and Γ_γ. For the Nevis column their published results were used. These were $\sigma_{t0}\Gamma^2$ *vs* Γ for the first six entries[22] and Γ_n and Γ_γ with $g=\frac{1}{2}$ for the last two entries.[4] For the lower energy resonances, the Nevis results were not quoted separately in reference 4. The Harwell σ_{t0} in Table II were calculated from their published values[19] of E_0, g, Γ_n and Γ. It is apparent from Table II that the present type of experiment and analysis gives quite satisfactory results over a large range of neutron energies.

[20] Seidl, Hughes, Palevsky, Levin, Kato, and Sjörstrand, Phys. Rev. **95**, 476 (1954).

[21] Fluharty, Simpson, and Simpson, Phys. Rev. **103**, 1778 (1956).

[22] E. Melkonian, Proceedings of the Conference on Neutron Physics by Time-of-Flight, Gatlinburg, Tennessee, 1956 [Oak Ridge National Laboratory Report ORNL-2309, 1957 (unpublished)].

ACKNOWLEDGMENTS

The contributions of Dr. C. P. Baker are acknowledged in providing the early forms of the pulsing and analysing equipment and as a source of helpful discussion during later developments and experiments. The aid of Mr. T. Eaton in early developments is acknowledged, and the assistance of Mr. M. Petruk in the construction, execution, and analysis of these experiments was indispensable. The cheerful cooperation of the BNL 60-in. cyclotron crew must also be recorded.